

Stable hybrid stars within a SU(3) Quark-Meson-Model

Andreas Zacchi,^{1,*} Matthias Hanauske,^{1,2,†} and Jürgen Schaffner-Bielich^{1,‡}

¹*Institut für Theoretische Physik, Goethe Universität Frankfurt,
Max von Laue Strasse 1, D-60438 Frankfurt, Germany*

²*Frankfurt Institute for Advanced Studies, Ruth-Moufang-Strasse 1, 60438 Frankfurt, Germany*
(Dated: October 18, 2018)

The inner regions of the most massive compact stellar objects might be occupied by a phase of quarks. Since the observations of the massive pulsars PSR J1614-2230 and of PSR J0348+0432 with about two solar masses, the equations of state constructing relativistic stellar models have to be constrained respecting these new limits. We discuss stable hybrid stars, i.e. compact objects with an outer layer composed of nuclear matter and with a core consisting of quark matter (QM). For the outer nuclear layer we utilize a density dependent nuclear equation of state and we use a chiral SU(3) Quark-Meson model with a vacuum energy pressure to describe the objects core. The appearance of a disconnected mass-radius branch emerging from the hybrid star branch implies the existence of a third family of compact stars, so called *twin* stars. Twin stars did not emerge as the transition pressure has to be relatively small with a large jump in energy density, which could not be satisfied within our approach. This is, among other reasons, due to the fact that the speed of sound in QM has to be relatively high, which can be accomplished by an increase of the repulsive coupling. This increase on the other hand yields too high transition pressures for twins stars to appear.

I. INTRODUCTION

A proto-compact star is formed in the aftermath of a supernova explosion, which is one of the most extreme events to occur in the universe. At low temperature and finite baryon density these objects contain the densest matter known to mankind, which exceeds even nuclear density ($\rho_0 \approx 2.5 \cdot 10^{14}$ g/cm³). The recent measurements of the massive pulsars PSR J1614-2230 [1] and of PSR J0348+0432 [2] with about two solar masses exceed the highest measured pulsar mass of PSR 1913+16 with $M \sim 1.44M_\odot$ by far [3]. This new mass limit sets constraints on the equation of state of dense matter within compact stellar objects. The repulsive effect of the strong interaction triples the maximum obtainable mass compared to a non-interacting Fermi gas of neutrons [4]. An appropriate EoS therefore should yield solutions for compact stars with $\gtrsim 2M_\odot$ and illustrates likewise the importance of the incorporated interactions. Spherically symmetric compact stars are generally described by the Tolman-Oppenheimer-Volkoff equations (TOV equations) [5]. These equations can be derived by solving the Einstein field equations

$$G_{\mu\nu} = R_{\mu\nu} - \frac{1}{2}Rg_{\mu\nu} = -\frac{8\pi G}{c^4}T_{\mu\nu} \quad (1)$$

where $G_{\mu\nu}$ is the Einstein tensor, $R_{\mu\nu}$ a contraction of the Riemann curvature tensor, called Ricci tensor, R being the curvature scalar and $T_{\mu\nu}$ the energy-momentum tensor of a relativistic fluid. Under the above mentioned

assumptions one arrives at

$$\frac{dm}{dr} = 4\pi r^2 \epsilon(r) \quad (2)$$

$$\frac{dp}{dr} = -\frac{\epsilon(r)m(r)}{r^2} \quad (3)$$

$$\cdot \left(1 + \frac{p(r)}{\epsilon(r)}\right) \left(1 + \frac{4\pi r^3 p(r)}{m(r)}\right) \left(1 - \frac{2m(r)}{r}\right)^{-1}$$

in units where $c = G = 1$.

The solutions of these equations are determined by different equations of state (EoS), and the entire collection of masses and corresponding radii is called the mass-radius relation (MR) of compact stars [6]. For each EoS, $p(\epsilon) = p(\epsilon(r))$, where p is the pressure and ϵ the corresponding energy density at a given radius r , exists a solution which is parametrized by p_c , the central pressure of the star.

Two different types of compact stars containing quark matter ought to be considered. The first one is based on the idea that the appearance of the strange quark lowers the energy per baryon and consequently forms the true ground state of nuclear matter, i.e. forms the whole star [7–9]. The resulting object is called a pure quark star and has been entirely discussed within the SU(3) model in [10]. The second one is called a hybrid star, where a quark matter (QM) core is surrounded by an outer crust of hadronic matter (HM). The transition from nuclear matter to quark matter can occur either in a mixed phase (Gibbs construction) or, assuming that there exists a first order phase transition at p_t , at a sharp transition (Maxwell construction).

Now, the particle transformations described by the EoS may influence the compressibility of the star, which can affect the stability. Is this effect significantly enough to alter the properties of the resulting compact object, i.e.

* zacchi@astro.uni-frankfurt.de

† hanauske@astro.uni-frankfurt.de

‡ schaffner@astro.uni-frankfurt.de

give rise to a third family of degenerate stars, so called *twin* stars? These objects would again be stable at a smaller radius but similar mass as the former compact star. A possible evidence of twin stars goes along with a discontinuity in the EoS. [11–19]. In this article we study various EoS and their solutions within the TOV equations using a Maxwell construction. A stable hybrid star configuration with $p_c \geq p_t$ is given, if the mass of the star continues to increase after the quark matter core appears [20–22]. As soon as the mass decreases with larger central pressures, the configurations become unstable. If the mass then, after decreasing, increases again with larger p_c , a stable twin star configuration would have been established. This behaviour is determined by the energy discontinuity $\Delta\epsilon$ between the two EoS and the speed of sound within the object. The works of Alford et. al [20–22] confirmed that a stable connected hybrid star branch emerges from the hadronic branch if the energy density discontinuity is less than a critical value. They used a constant speed of sound parametrization within the fields correlator method for the QM EoS to provide a general framework for empirical testing and comparison. The recent observations of the $2M_\odot$ -stars [1, 2] constraints the constant speed of sound parametrization. A stiffer HM EoS and $c_s^2 \geq \frac{1}{3}$ for the QM EoS yields solutions with star sequences $\geq 2M_\odot$ in their approach. In this work we will work with a density dependent (DD2) nuclear matter EoS [23] for the outer layers of the star and a chiral SU(3) EoS derived from the Quark-Meson model [10] for the stars core. In [10] pure quark star configurations $\geq 2M_\odot$ for a small parameter rage were found, in this model all other solutions were hybrid stars completely buildt of a mixed phase of HM and QM. We scan the same parameters of the SU(3) EoS as in [10] to look for possible twin stars emerging from a stable hybrid star.

II. THE MODELS

According to lattice QCD calculations, the phase transition at high baryonic densities is of first order [24–26]. Based on this assumption the transition from hadronic matter to quark matter is described via a Maxwell construction [27–29]. The quark-meson model couples mesons as mediators of the strong interaction to quarks utilizing chiral symmetry [30] via a Yukawa type coupling. The coupled equations of motions of the meson fields derived from the grand canonical potential have to be solved self-consistently and determine finally the EoS. Possible resulting pure quark stars emerging from the chiral SU(3) Quark Meson model have been discussed entirely in [10] such as the derivation of the EoS.

1. Chiral Quark Meson Model

The SU(3) Lagrangian \mathcal{L} of the chiral quark-meson model reads

$$\begin{aligned} \mathcal{L} = & \bar{\Psi} (i\not{\partial} - g_\varphi\varphi - g_v\gamma^\mu V_\mu) \Psi \\ & + tr(\partial_\mu\varphi)^\dagger(\partial^\mu\varphi) + tr(\partial_\mu V)^\dagger(\partial^\mu V) \\ & - \lambda_1[tr(\varphi^\dagger\varphi)]^2 - \lambda_2 tr(\varphi^\dagger\varphi)^2 \\ & - m_0^2(tr(\varphi^\dagger\varphi)) - m_v^2(tr(V^\dagger V)) \\ & - tr[\hat{H}(\varphi + \varphi^\dagger)] + c(\det(\varphi^\dagger) + \det(\varphi)) \end{aligned} \quad (4)$$

for $SU(3) \times SU(3)$ chiral symmetry incorporating the scalar (φ) and vector (V_μ) meson nonet. Here, m_v stands for the vacuum mass of the vector mesons and λ_1 , λ_2 , m_0 , and c are the standard parameters of the linear σ model [30–33]. The matrix \hat{H} describes the explicit breaking of chiral symmetry. The quarks couple to the meson fields via Yukawa-type interaction terms with the couplings strengths g_φ and g_v for scalar and vector mesons, respectively.

The energy density and the pressure are then determined to

$$\begin{aligned} \epsilon = & \epsilon_e + \frac{\lambda_1}{4}(\sigma_n^2 + \sigma_s^2)^2 + \frac{\lambda_2}{4}(\sigma_n^4 + \sigma_s^4) \\ & + \frac{m_0^2}{2}(\sigma_n^2 + \sigma_s^2) - \frac{2\sigma_n^2\sigma_s}{\sqrt{2}} \cdot c - h_n\sigma_n - h_s\sigma_s + B \\ & + \frac{1}{2}(m_\omega^2\omega^2 + m_\rho^2\rho^2 + m_\phi^2\phi^2) \\ & + \frac{3}{\pi^2} \sum_{f=u,d,s} \int_0^{k_F^f} dk \cdot k^2 \left(\sqrt{k_{n,s}^2 + \tilde{m}^2} \right) \end{aligned} \quad (5)$$

and

$$\begin{aligned} p = & -\frac{1}{2}(m_\omega^2\omega^2 + m_\rho^2\rho^2 + m_\phi^2\phi^2) \\ & + \frac{\lambda_1}{4}(\sigma_n^2 + \sigma_s^2)^2 + \frac{\lambda_2}{4}(\sigma_n^4 + \sigma_s^4) \\ & + \frac{m_0^2}{2}(\sigma_n^2 + \sigma_s^2) - \frac{2\sigma_n^2\sigma_s}{\sqrt{2}} \cdot c - h_n\sigma_n - h_s\sigma_s + B \\ & + \frac{3}{\pi^2} \sum_{f=u,d,s} \int_0^{k_F^f} dk \cdot k^2 \left(\sqrt{k_{n,s}^2 + \tilde{m}^2} - \tilde{\mu}_f \right) \end{aligned} \quad (6)$$

where the indices n=nonstrange (up- and down quarks) and s=strange quarks. For the couplings and masses of the included fields standard values are assumed. A detailed treatment on the parameters can be found in [10, 30, 32, 34]. Since the properties of the reviewed hybrid stars depends only on the parameters of the quark sector, a broader overview shall be given compared to the nuclear matter parameter range. However, four parameters can be varied:

1. The constituent quark mass m_q determines the scalar coupling for the nonstrange g_n and strange condensate g_s via the Goldberger-Treiman relation:

$g_n = \frac{m_q}{f_\pi}$ and $g_s = g_n\sqrt{2}$, where g_s is adopted from SU(3) symmetry considerations.

2. The vector coupling is independent of the constituent quark mass, it will be varied in the scale of the scalar coupling, $g_\omega \sim g_n$, to study its influences in an appropriate range. The strange coupling of the ϕ -meson is fixed by SU(3) symmetry.
3. The experimentally not well determined mass of the σ -meson covers a range from $400 \text{ MeV} \leq m_\sigma \leq 800 \text{ MeV}$ [35, 36].
4. The Bag constant B models the confinement and can be interpreted as a vacuum energy density term. The fields are independent of its variation, its impact is to stiffen or soften the EoS. Physically reasonable ranges within this context are $60 \text{ MeV} \leq B^{\frac{1}{4}} \leq 200 \text{ MeV}$.

III. HYBRID STARS

At large densities hadronic matter is expected to undergo two phase transitions. The first one deconfines hadrons to quarks and gluons. Note that in a strict sense neither the deconfinement phase transition nor the chiral phase transition can be described by an order parameter based on underlying symmetries of QCD. The second one restores chiral symmetry. Yet it is an unsettled issue whether these transitions are real phase transitions or crossover transitions [37]. We will study and compare various models at ultrahigh densities to search for differences and similarities as well as their resulting predictions for compact objects, i.e. the mass-radius relation.

A. Construction of the phase transition

The study of the deconfined phase transition is related to the mixed phase. It has been suggested, that the mixed phase in compact objects behaves more in accordance with the Maxwell construction than with the Gibbs construction [29, 38, 39]. Furthermore it is more likely that twin stars appear within the Maxwell construction, according to [29]. In this article we thus utilize a Maxwell construction due to the above mentioned reasons. In refs [20–22] the QM EoS was parametrized a relatively simple form (see eq. 11) and the transition from HM to QM can be constructed without any constraints concerning the chemical potential. Our approach on the other hand needs to take into account the pressure as function of the chemical potential to find the thermodynamically justified transition pressure (see fig. 11 and the discussion there).

In electrically neutral stellar matter baryon number and charge have to be conserved quantities. Under this assumption the chemical potential of species i can be de-

finied as

$$\mu_i = B_i\mu_B + Q_i\mu_Q \quad (7)$$

where B_i is the baryon number and Q_i the charge in units of the electron charge and μ_B and μ_Q are the baryonic and electric chemical potentials respectively. Note, that strangeness is not a conserved quantity. The phase transition from HM to QM produces a mixed phase. Now, the Gibbs condition requires that the coexisting phases have opposite charge and it might also happen that the mixed phase is energetically too expensive [29, 38]. Then the two phases are in direct contact with each other, which corresponds to a Maxwell construction, where

$$P_{HM}(\mu_B, \mu_Q) = P_{QM}(\mu_B, \mu_Q) \quad (8)$$

$$\mu_B = \mu_{HM} = \mu_{QM} \quad (9)$$

The baryon chemical potential is continuous, but μ_Q jumps at the interface of the two phases, so that the phase transition takes place if the pressure of the QM phase equals the pressure of the HM phase at a given baryo-chemical potential μ_B . The MC corresponds to constant pressure in the energy density interval of the mixed phase, whereas the pressure increases with baryon density in the GC.

However, the existence of a quark phase in a compact star requires the transition pressure to be smaller than the central pressure of the star, which is valid for the MC and also for the GC.

B. Stability Criteria

As long as the mass of the star is an increasing function of p_c the compact object will be stable. Since a hybrid star contains a QM-core, there exists a threshold value in the jump in energy density $\Delta\epsilon_c$ which determines the stars stability when the QM-core first appears.

$$\frac{\Delta\epsilon_c}{\epsilon_t} = \frac{1}{2} + \frac{3p_t}{2\epsilon_t} \quad (10)$$

where ϵ_t and p_t are the values of the energy density and pressure at the phase transition. For a derivation and discussion of (10) see [11–14, 40–43].

For a high value of $\Delta\epsilon$ the cusp in the MR relation is hardly detectable and in the range of $\sim 10^{-4}M_\odot$ in agreement with [19, 20, 43], i.e. shortly after the QM core appears the QM core is unable to counteract the gravitational attraction from the HM and the star becomes unstable.

IV. RESULTS

The appearance of a QM core within a compact star is entirely determined by the transition pressure p_t and the discontinuity in the energy density $\Delta\epsilon$. If the pressure

within the star lies below the transition pressure, the object would be entirely determined by the HM EoS and could not be classified as a hybrid star. The relation $\frac{\Delta\epsilon}{\epsilon_t}$ as a function of $\frac{p_t}{\epsilon_t}$ will become important in context with eq. (10) when investigating for connected or disconnected hybrid star branches [20–22].

A. Various EoS and the corresponding mass-radius relations for fixed B and different g_ω

Figure 1 shows the total hybrid EoS for a fixed value of the vacuum pressure $B = 60$ MeV while varying the vector coupling constant from $0 \leq g_\omega \leq 3$.

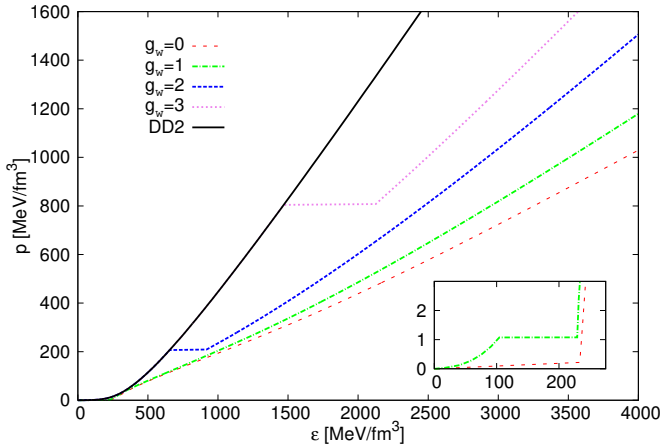


FIG. 1. The EoS with fixed $B = 60$ MeV while varying g_ω at $m_\sigma = 600$ MeV and $m_\rho = 300$ MeV. The inlaid figure accentuates the behaviour of the EoS for $g_\omega = 0$ and $g_\omega = 1$ which else is hardly perceivable.

For increasing values of the repulsive coupling the transition pressure p_t increases due to a stiffening in the QM EoS.

The $g_\omega = 0$ case corresponds to a transition from HM to QM at $\frac{p_t}{\epsilon_0} \leq 1$. A transition occurring below saturation energy density is clearly unphysical and shall therefore not be discussed any further (see upper x axis in fig 10). For $g_\omega = 1$ the transition occurs at $p_t \simeq 1.5$ MeV/fm³ and $\epsilon_t \simeq 102$ MeV/fm³ (see inlaid figure in fig. 1). The discontinuity in energy density here is $\Delta\epsilon \simeq 122$ MeV/fm³. In this case $\frac{\epsilon}{\epsilon_0} \simeq 1$, see also fig. 10, which corresponds to the leftmost data point on the $g_\omega = 0$ line. Note that in fig. 1 and in all following graphics the pure HM results are shown as a reference, denoted as “DD2”.

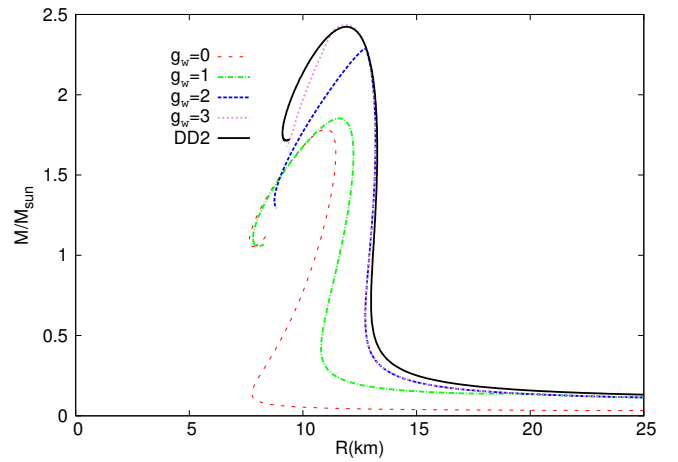


FIG. 2. The mass-radius relation with fixed $B = 60$ MeV while varying g_ω at $m_\sigma = 600$ MeV and $m_\rho = 300$ MeV.

The corresponding mass-radius relation is shown in fig. 2. For $g_\omega = 1$ the phase transition from HM to QM does not destabilize the star for a relatively wide range in mass, i.e. the emerging QM core gets larger while the hybrid star manages to stay stable up to $\sim 1.7M_\odot$. This behaviour is very similar to the one of the hadronic mode “DD2”, but shifted to smaller masses and radii.

A repulsive coupling of $g_\omega = 2$ on the other hand results in a connected hybrid star branch hardly detectable compared to $g_\omega = 1$ and with a similar trend as the “DD2” case, but with solutions reaching $\gtrsim 2M_\odot$.

For $g_\omega = 3$ the transition sets in at already unstable configurations for the pure nuclear matter case.

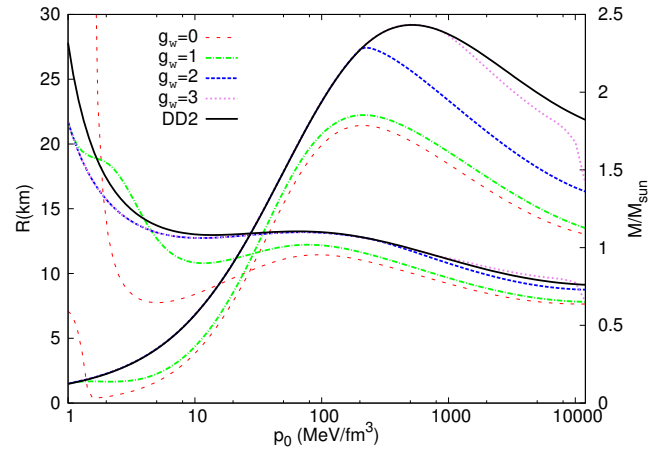


FIG. 3. The radius- and mass curves as function of p_c with fixed $B = 60$ MeV while varying g_ω at $m_\sigma = 600$ MeV and $m_\rho = 300$ MeV. The curves starting in the upper left region are the radius curves whereas the curves starting on the lower left side are the mass curves.

Figure 3 displays the radius- and mass curves as function of p_c with $B \geq 60$ MeV while varying g_ω at $m_\sigma = 600$ MeV and $m_\rho = 300$ MeV. The curves starting in the

upper left region are the radius curves for a given value of g_ω . The curves starting on the lower left side are the mass curves. The associated x-axis in fig. 3 shows the pressure pertaining to both curves. The curves leave the hadronic “DD2” reference line at the respective transition pressure p_t and, still rising, yielding stable hybrid star solutions. Unstable solutions can be read off from the point on where the mass decreases with increasing pressure. These features are valid for all following radius- and mass curves as function of p_c .

Figure 3 substantiates the hitherto discussion regarding the increase of the repulsive coupling by depicting up to which central pressure the hybrid star configurations stay stable: With higher repulsive coupling, the appearing hybrid star configurations become unstable, i.e. the smaller the resulting QM core, though the masses are significantly higher.

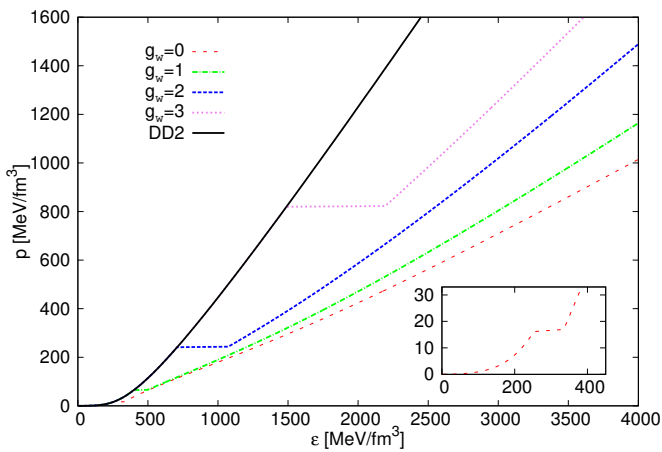


FIG. 4. The EoS with fixed $B = 100$ MeV while varying g_ω at $m_\sigma = 600$ MeV and $m_\rho = 300$ MeV. The inlaid figure shows the behaviour of the EoS for $g_\omega = 0$.

Figure 4 shows the EoS for $B = 100$ MeV. The transition pressure increases with an associate increase of the jump in energy density.

For $g_\omega = 0$ with fixed $B = 100$ MeV the respective values are $p_t \simeq 15$ MeV/fm³, $\epsilon_t \simeq 230$ MeV and $\Delta\epsilon \simeq 90$ MeV/fm³, see inlaid figure in figure 4 and see fig. 10 for $\frac{\epsilon}{\epsilon_0} \simeq 1.8$ respectively.

For $g_\omega = 1$ and $B = 100$ MeV we find $p_t \simeq 75$ MeV/fm³, $\epsilon_t \simeq 380$ MeV/fm³ and $\Delta\epsilon \simeq 100$ MeV/fm³ at $\frac{\epsilon}{\epsilon_0} \simeq 2.8$, see also fig. 10.

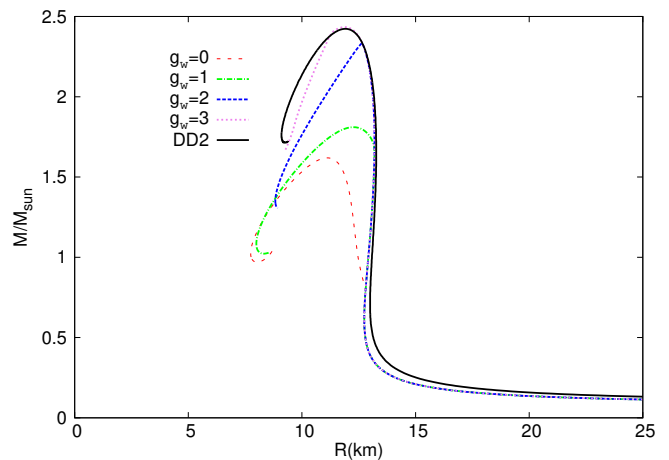


FIG. 5. The mass-radius relation with fixed $B = 100$ MeV while varying g_ω at $m_\sigma = 600$ MeV and $m_\rho = 300$ MeV.

The resulting mass-radius relations for these EoS are shown in fig. 5. Increasing further the repulsive coupling leads to hybrid star configurations, which do not support a stable QM core ($g_\omega \geq 2$). The trends of the curves obviously show differences to the $B = 60$ MeV parameter choice. The transition pressures for $B = 100$ MeV are higher compared to the $B = 60$ MeV case, see figs. 3 and 6, and the appearing QM core does destabilize the configurations.

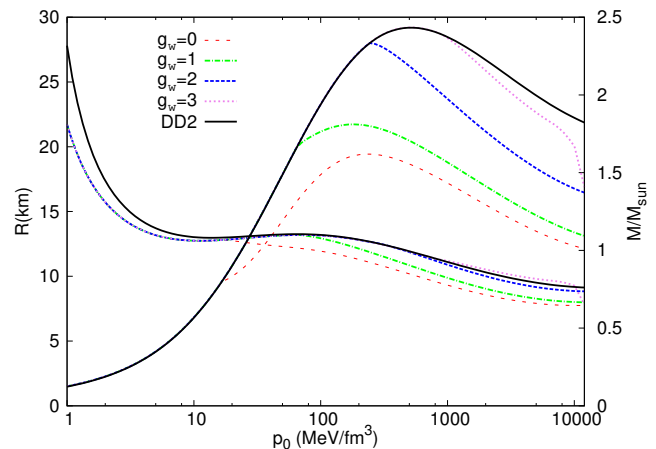


FIG. 6. The radius- and mass curves as function of p_c with fixed $B = 100$ MeV while varying g_ω at $m_\sigma = 600$ MeV and $m_\rho = 300$ MeV. The curves starting in the upper left region are the radius curves whereas the curves starting on the lower left side are the mass curves.

The QM core for $g_\omega = 0$ appears at $\sim 0.8M_\odot$ at a radius of ~ 12.5 km, see fig. 6 where the mass and radius lines leaves the hadronic “DD2” reference line. The star does not get unstable up to $\sim 1.6M_\odot$ at a radius of ~ 11 km.

The QM core for $g_\omega = 1$ appears at $\sim 1.6M_\odot$. The hybrid star configurations stay stable up to $\sim 1.7M_\odot$,

see figs. 5 and 6. The appearance of the QM core at $g_\omega = 1$ destabilizes the star configurations faster than in the $g_\omega = 0$ case for $B = 100$ MeV. The EoS for $B = 140$ MeV is shown in fig. 7. It shows an increase of the transition pressure p_t as expected.

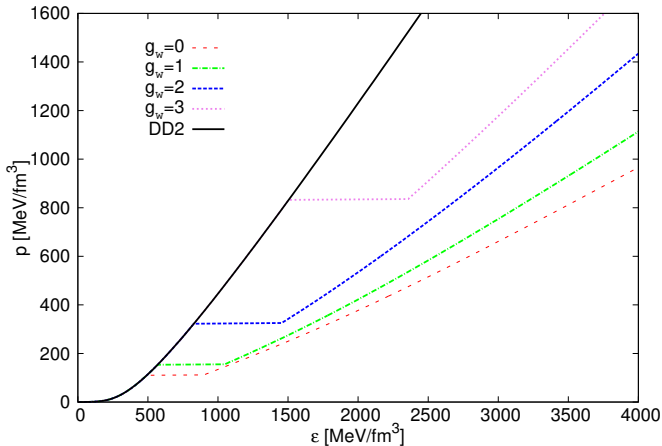


FIG. 7. The EoS with fixed $B = 140$ MeV while varying g_ω at $m_\sigma = 600$ MeV and $m_q = 300$ MeV.

The discontinuity in energy density increases too, but displays a nontrivial relation to p_t which can be observed in greater detail in the phase diagram shown in fig. 10.

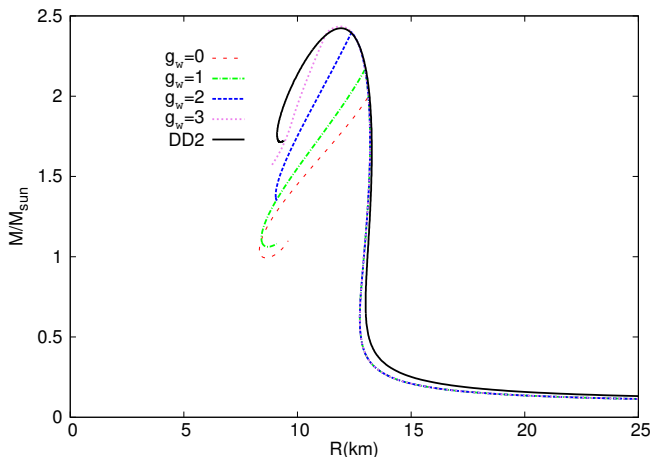


FIG. 8. The mass-radius relation with fixed $B = 140$ MeV while varying g_ω at $m_\sigma = 600$ MeV and $m_q = 300$ MeV.

The resulting mass-radius curve for $B = 140$ MeV is shown in fig. 8. A hybrid star branch appears but is hardly noticeable. As already mentioned, the transitions for a value of $g_\omega = 3$ sets in at an already unstable configurations, i.e. no stable hybrid star branch at all emerges.

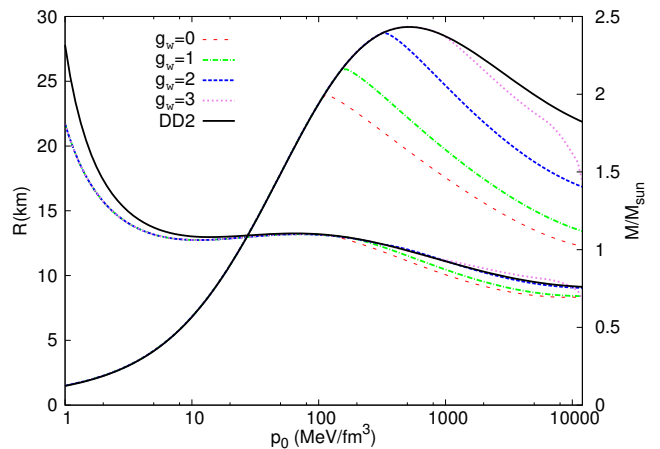


FIG. 9. The radius- and mass curves as function of p_c with fixed $B = 140$ MeV while varying g_ω at $m_\sigma = 600$ MeV and $m_q = 300$ MeV. The curves starting in the upper left region are the radius curves whereas the curves starting on the lower left side are the mass curves.

Fig. 9 shows the corresponding radius- and mass curve as function of the central pressure. The hybrid star configurations follow the “DD2” curve, and become unstable nearly immediately after the appearance of the QM core. The repulsive force in the QM EoS is not strong enough to support a large hadronic mantle. The star would collapse having a too large QM core.

Generally speaking: Raising the value of the vacuum pressure leads to hybrid star branches where the hybrid stars destabilize faster after the appearance of the QM core, and the transition occurs at higher masses.

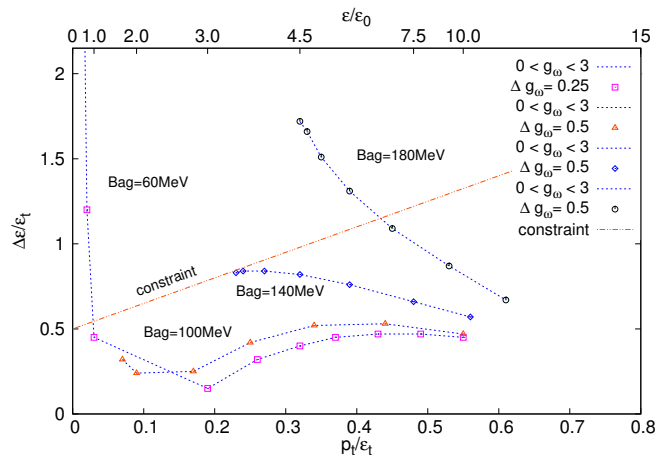


FIG. 10. Phase diagram for hybrid stars with fixed B while varying $0 \leq g_\omega \leq 3$ at constant $m_\sigma = 600$ MeV and $m_q = 300$ MeV. The axes display the transition pressure p_t and the energy density discontinuity $\Delta\epsilon$ in units of the nuclear energy density at the transition ϵ_t . Note, that the first data point for the $B = 60$ MeV line (on the left) corresponds to $g_\omega = 1$. The following data points are incremented by $\Delta g_\omega = 0.25$.

The phase diagram displayed in figure 10 depicts the

ratio of pressure to energy density at the transition of hadronic matter versus the discontinuity in energy density at the transition. The upper x axis displays the corresponding central energy density in units of nuclear energy density $\epsilon_0 \simeq 145 \frac{\text{MeV}}{\text{fm}^3}$.

The transition for small values of B and g_ω occurs at a too small central energy density $\frac{\epsilon_t}{\epsilon_0} \leq 1$. For large values of B and a small repulsive coupling the transition occurs at 4 – 10 times nuclear saturation density. Within the range $100 \leq B \leq 140$ MeV the transition for zero repulsion stays below the constraint line, given by eqn. 10. It is interesting to note that all curves converge in an area at around $0.55 \leq \frac{p_t}{\epsilon_t} \leq 0.65$ and $0.4 \leq \frac{\Delta\epsilon}{\epsilon_t} \leq 0.6$ where the central energy density is ~ 10 times nuclear saturation density (even for higher values of g_ω not displayed here). Figure 11 displays the pressure as a function of the chemical potential μ for the parameter choice $m_\sigma = 600$ MeV, $m_q = 300$ MeV and $B = 100$ MeV while varying $0 \leq g_\omega \leq 3$. The intersecting point between the HM-and the QM curve indicates where the transition pressure for a given choice of parameters is located.

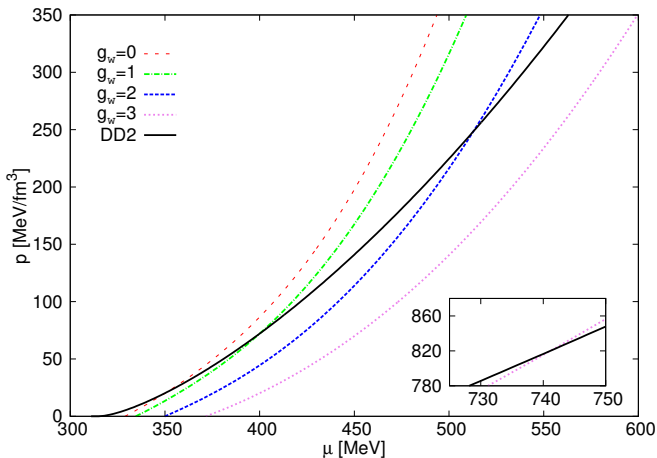


FIG. 11. The intersection in the pressure versus chemical potential μ plane for $0 \leq g_\omega \leq 3$ within the parameter choice $m_\sigma = 600$ MeV, $m_q = 300$ MeV and $B = 100$ MeV, corresponding to figs. 4, 5 and 6. The MC requires that from the intersecting point on the dominance in the EoS flips, which creates a QM core within the star at the corresponding pressure.

The inlaid figure shows the intersection for the $g_\omega = 3$ case, which is out of the plot range.

The intersection for $g_\omega = 0$ takes place at $p \simeq 15$ MeV/fm³ and $\mu \simeq 355$ MeV and for $g_\omega = 1$ at $p \simeq 75$ MeV/fm³ and $\mu \simeq 400$ MeV, see also figs. 4 and 6. It is interesting to note that the a stiffer EoS has a “softer” behaviour in the $p - \mu$ plane. Softer means here that for larger values of g_ω both, pressure and μ increase, i.e. the intersection takes place at a higher pressure. That corresponds to a transition from HM to QM at a higher central energy density in terms of nuclear energy density, see figs. 10 and 16 for comparison (upper x-axis). An appearing QM core destabilizes the star

quite soon, and twin star solutions are ruled out, since these require a relatively low transition pressure [19, 26].

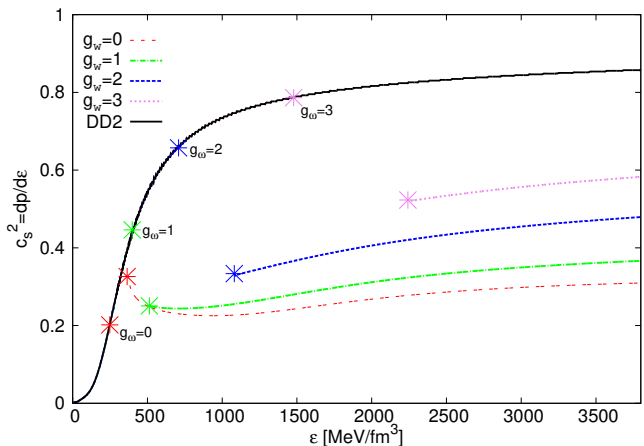


FIG. 12. The speed of sound $c_s^2 = \frac{dp}{d\epsilon}$ as a function of the energy density ϵ for $0 \leq g_\omega \leq 3$ within the parameter choice $m_\sigma = 600$ MeV, $m_q = 300$ MeV and $B = 100$ MeV, corresponding to figs. 4, 5 and 6. For this parameter choice the transition is marked by the symbols on the “DD2” curve.

In fig. 12 we examine the speed of sound for $0 \leq g_\omega \leq 3$ within the parameter choice $m_\sigma = 600$ MeV, $m_q = 300$ MeV and $B = 100$ MeV, corresponding to figs. 4, 5 and 6. Since the Bag constant does not affect the stiffness of the EoS (it just changes the value of the vacuum pressure) the slope of these curves for any choice of B would remain the same. Only the transition values of the energy density ϵ_t from one EoS to the other EoS would change and in equal steps of $\Delta\epsilon$.

For $g_\omega = 0$ and $g_\omega = 1$, $\Delta\epsilon \simeq 95$ MeV/fm³, see also the discussion in the previous sections. The symbols on the “DD2” curve mark the point where the transition takes place and the stars leave the hadronic branch. The corresponding symbols on the QM lines mark then the points, where the QM core appears. As one would expect, an increase of the repulsive coupling not only stiffens the EoS but also raises the speed of sound within the medium. The $g_\omega = 0$ line saturates at $c_s^2 = \frac{1}{3}$ which is reasonable since ultrarelativistic matter without interactions saturates at $p(\epsilon) = \frac{1}{3}\epsilon$ [44, 45]. Since $g_\omega = 3$ has far too high transition pressures for hybrid- and twin stars the highest considered repulsive coupling $g_\omega = 2$ reaches $c_s^2 \simeq 0.5$. That means that all physically relevant and considered cases in this work lie within $0.3 \leq c_s^2 \leq 0.5$. This will become important in the following when we compare our results with those from Alford et. al [20–22].

B. Various EoS and the corresponding mass-radius relations for fixed g_ω and different B

Figure 13 shows the EoS at fixed $g_\omega = 0$ for various values of the Bag constant B . For increasing values of

B the transition pressure p_t increases. As in the case of increasing B at fixed g_ω , increasing B while varying g_ω leads to the same behaviour of the different EoS.

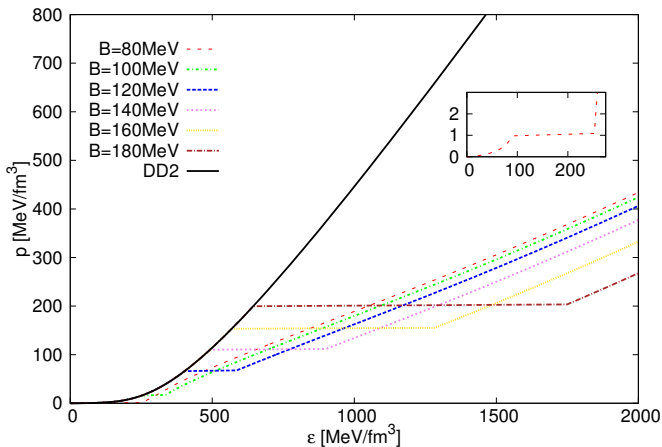


FIG. 13. The EoS with fixed $g_\omega = 0$ while varying B at $m_\sigma = 600$ MeV and $m_q = 300$ MeV. The inlaid figure shows the behaviour of the EoS for $B = 180$ MeV.

For $B = 80$ MeV $p_t \simeq 1$ MeV/fm³, $\epsilon_t \simeq 92$ MeV/fm³ and the discontinuity in energy density is $\Delta\epsilon \simeq 160$ MeV/fm³ (see inlaid figure). For the highest chosen value of $B = 180$ MeV $p_t \simeq 202$ MeV/fm³, $\epsilon_t \simeq 650$ MeV/fm³ and $\Delta\epsilon \simeq 1100$ MeV/fm³, i.e. the discontinuity in the energy density $\Delta\epsilon$ increases also with B .

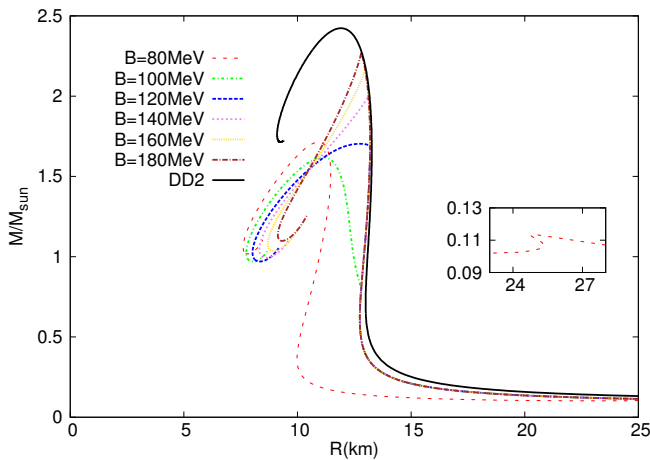


FIG. 14. The mass-radius relation with fixed $g_\omega = 0$ while varying B at $m_\sigma = 600$ MeV and $m_q = 300$ MeV. The inlaid figure accentuates the behaviour of the mass-radius curve for $B = 80$ MeV which else is hardly perceivable.

Figure 14 shows the mass-radius relations for $g_\omega = 0$ while varying B with $m_\sigma = 600$ MeV and $m_q = 300$ MeV. For the smallest value of $B = 80$ MeV the QM core appears at already $0.11M_\odot$ at a radius of ~ 25 km (see inlaid figure), see also fig. 15. The shape of the curve is

similar to the pure hadronic one but shifted to slightly smaller values of mass and radius due to the appearance of the QM core. The transition from HM to QM appears at $\frac{\epsilon}{\epsilon_0} \leq 1$, see fig. 16. The inlaid figure displays a disconnected mass-radius branch, which is an indication for a twin star. These disconnected solutions were found up to values of $B \simeq 90$ MeV, getting harder to detect with larger B and always at physically too small transition energy densities $0.66 \leq \frac{\epsilon}{\epsilon_0} \leq 1$, see figs. 16 and 20, and shall therefore not be discussed any further.

For $B = 100$ MeV the transition occurs at $\frac{\epsilon}{\epsilon_0} \simeq 1.8$. The respective values are $p_t \simeq 15$ MeV/fm³, $\epsilon_t \simeq 230$ MeV/fm³ and $\Delta\epsilon \simeq 90$ MeV/fm³ (see also inlaid figure in fig. 4, fig. 13 and fig. 15). The QM core appears at $\sim 0.8M_\odot$ at a radius of ~ 12.5 km. The star configuration does not get unstable up to $\sim 1.6M_\odot$ at a radius of ~ 11 km, which can altogether be observed in fig. 15. The resulting mass-radius relation for this EoS is also shown in fig. 5. Higher values of the vacuum energy term B lead to much smaller hybrid star branches, hardly visible and in accordance with [20–22]. The configurations get unstable nearly immediately after the appearance of the QM core, which itself emerges at a higher mass.

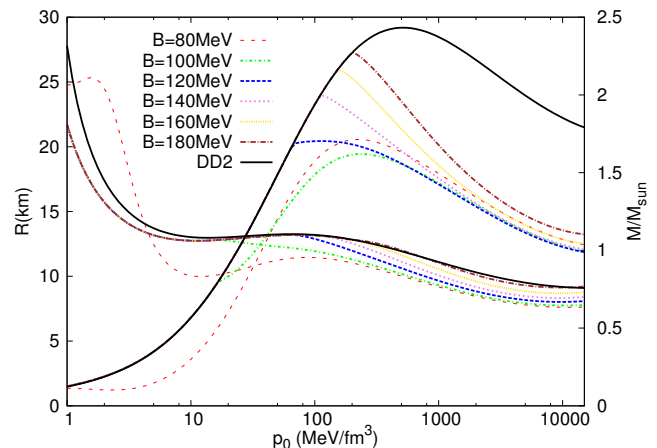


FIG. 15. The radius- and mass curves as function of p_c with fixed $g_\omega = 0$ while varying B at $m_\sigma = 600$ MeV and $m_q = 300$ MeV. The curves starting in the upper left region are the radius curves whereas the curves starting on the lower left side are the mass curves.

The case $B = 140$ MeV reaches $\sim 1.9M_\odot$ but after the transition has set in, the star configurations get quickly unstable. These stars support, if they support, only a very small QM core and subsequently become unstable. However, the transition pressure rises with the increase of g_ω , which generates eventually an unstable QM core.

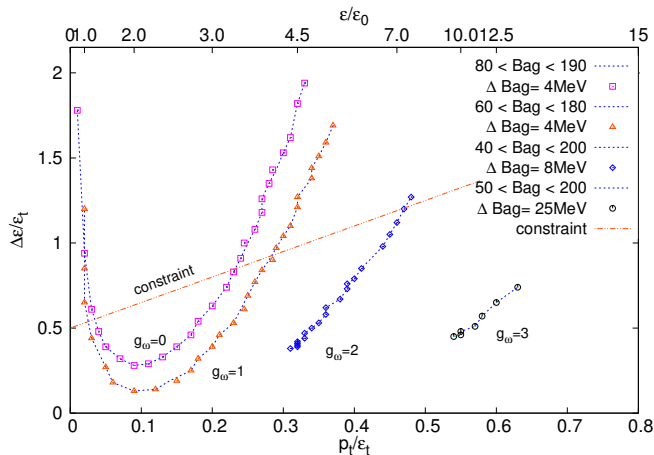


FIG. 16. Phase diagram for hybrid stars with fixed g_ω while varying $40 \text{ MeV} \leq B \leq 200 \text{ MeV}$ at constant $m_\sigma = 600 \text{ MeV}$ and $m_q = 300 \text{ MeV}$. The axes display the transition pressure p_t and the energy density discontinuity $\Delta\epsilon$ in units of the nuclear energy density at the transition ϵ_t .

The labelling of the axes in the phase diagram for fixed g_ω in fig. 16 is the same as for fixed B in fig. 10. Generally, increasing the value of the repulsive coupling of the QM EoS leads to a higher p_t and also a larger discontinuity $\Delta\epsilon$ for a given B . The higher the repulsive force within the QM core, the higher is p_t for a QM core to appear. For the transition to occur at $2\epsilon_0$, B has to be at least 104 MeV in case of zero repulsion ($g_\omega = 0$), corresponding to the minimum of the plotted data in fig. 16. For $g_\omega = 1$, B has to be at least 84 MeV to be located at $2\epsilon_0$. Both cases lead to stable hybrid star configurations, shown in figs. 14 and 15 for $g_\omega = 0$.

However, both trends are parabola like, crossing the constraint line twice, whereas the $g_\omega = 2$ and the $g_\omega = 3$ case stay below the constraint (except for the choice $g_\omega = 2$ and $B \gtrsim 190 \text{ MeV}$). The $g_\omega = 2$ case in the range $50 < B < 200 \text{ MeV}$ corresponds to $4.5 \leq \epsilon_t \leq 7$. There a connected hybrid star branch, even if very small and hardly observable, exists up to $B \simeq 180 \text{ MeV}$. The stars get unstable almost immediately after the appearance of the QM core. A higher value of B leads to transitions at already unstable mass-radius configurations. In case of even higher repulsion $g_\omega = 3$ the transition takes place not before 10 - 14 times nuclear energy density at an already unstable mass-radius configuration. Our results match the results from [20–22].

An investigation in the phase space by variation of m_σ and m_q lead us to the conclusion that neither $\frac{\Delta\epsilon}{\epsilon_t}$ nor $\frac{p_t}{\epsilon_t}$ changes in an adequate amount to get a relatively large jump in energy density accompanied with a small transition pressure, which is an essential requirement for twin stars, see fig. 20. Their attractive character through varying both quantities is far weaker than the variation of g_ω and B [10, 46, 47].

V. COMPARISON WITH OTHER MODELS

In the last section we have analyzed the parameter dependence of the resulting hybrid star properties within our HM-QM model. One main outcome of our analysis is the absence of a twin star region within the physical reasonable parameter space. Theoretically we have found a narrow parameter region where twin stars do exist ($p_t/\epsilon_t < 0.05$), however, within all of these EoSs the HM to QM phase transition appears at irrelevant low density values ($\epsilon_t < \epsilon_0$). As the existence of twin stars have been found in many different kind of phase-transition scenarios, e.g. hadron-quark phase transition [28, 48, 49] (using a Maxwell- or Gibbs construction), hyperon phase transition [50], pion [51] and kaon condensation [52, 53], the question arises, what the main reason is, that we do not find twins in our model? On the one hand, in all the existing twin star models, the relevant EoS parameter region where twins occur, is always narrow and a 'parameter fine-tuning' is needed to achieve an EoS which will result in a twin star behaviour. On the other hand, we have carefully analysed the allowed parameter space in the last section and did not find a twin star solutions where $\epsilon_t > \epsilon_0$.

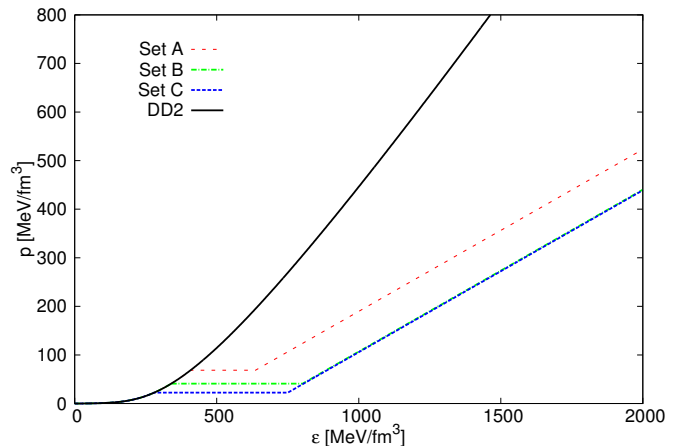


FIG. 17. The EoS for three different parameter sets corresponding to a QM-EoS given by eq. 11. The parameters of the three sets are displayed in table I.

We show that the non-existence of twin stars in our model is due to the fact that the potential twin star area lies outside of our available parameter region and therefore cannot be reached in our simulations. By constructing the phase transition within our model we are not capable to choose arbitrary values for $\Delta\epsilon$, ϵ_t and p_t (like Alford et. al [20–22]), because we need to match the HM-EoS with the QM-EoS in a consistent way, i.e. find the intersection between pressure p and chemical potential μ for the transition pressure p_t .

Star sequence	p_t/ϵ_t	$\Delta\epsilon/\epsilon_t$	M_1	R_1	M_2	R_2
● Set A	0.168	0.56	1.69332	13.262	1.69794	11.722
■ Set B	0.12	1.36	1.34586	13.208	1.26019	8.906
▲ Set C	0.08	1.68	0.96196	13.052	1.19709	7.893

TABLE I. *The parameter choice for a constant speed of sound $c_s^2 = \frac{1}{3}$ of the three different sets of star sequences with the respective masses and radii of the corresponding branches (fig. 18)*

In this section we use the same density dependent DD2 EoS for the hadronic part, but we use a much simpler model for the QM sector. Similar to [20–22] we take a QM-EoS, which is parameterized by the following three values: p_t , $\Delta\epsilon$ and c_s (constant sound speed in quark matter) and which is given by eq. 11. In order to construct a comparable QM-EoS with respect to our model, we have used a fixed value of $c_s^2 = 1/3$ for the following calculations. The EoS for $p > p_t$ in this simple QM model has the following form [20, 54]

$$p(\epsilon) = c_s^2(\epsilon - \epsilon_*) , \quad \text{with: } \epsilon_* := \epsilon_t + \Delta\epsilon - \frac{1}{c_s^2}p_t, \quad (11)$$

where ϵ_* is the energy density at zero pressure. Fig. 17 shows the resulting EoSs for three choices of the parameters, which are given in tab. I. In contrast to our model the parameters can be chosen in such a way that twin stars appear in a physically meaningful region.

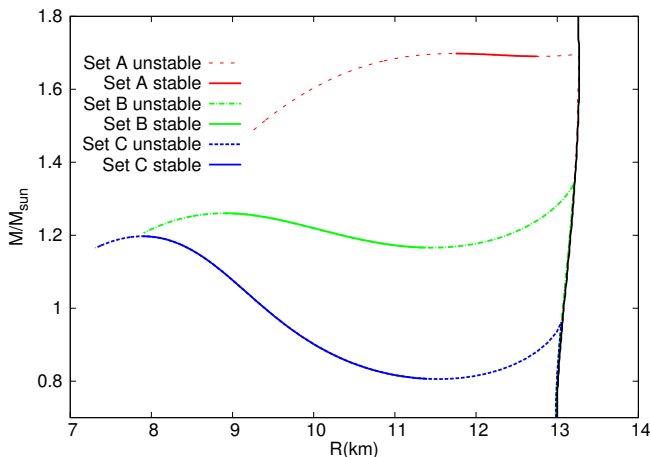


FIG. 18. *The mass-radius relation for three different parameter sets corresponding to a QM-EoS given by eq. 11. The parameters of the three sets are displayed in tab. I. Set C shows impressive the appearance of a second stable branch, where $M_2 > M_1$: The maximum mass of the second branch is larger than the maximum mass of the first branch. All displayed solutions are twin star solutions.*

In Figs. 18 and 19 the mass-radius relations and the radius-mass curves of the three chosen representative twin star parametrizations are displayed. The Set A

mass-radius relation has been calculated by using the parameter configuration: $\Delta\epsilon/\epsilon_t = 0.56$ and $p_t/\epsilon_t = 0.168$, which is located below the constraint-line given by eq. 10 (see fig. 20). This configuration is located right at the corner of the twin star region boundary lines and the differences between the maximum masses of the first and second sequence is very small ($M_1^{max} = 1.69332M_\odot$ and $M_2^{max} = 1.69794M_\odot$). Set B displays a twin star where the first sequence maximum mass lies above the maximum mass of the twin star ($\Delta\epsilon/\epsilon_t = 1.36$, $p_t/\epsilon_t = 0.12$). The Parameter Set C curve shows the mass-radius relation of a twin star sequence with a rather high value of $\Delta\epsilon/\epsilon_t = 1.68$ but a low value of $p_t/\epsilon_t = 0.08$. The phase transition starts at low density and the maximum mass of the first sequence is much lower than the maximum mass of the twin star sequence (see table I). In this model too the neutron star sequence continuously moves to the hybrid star branch and hybrid stars with a tiny quark core are stable for a short period. The connected stable hybrid star branch is very small and difficult to recognize, as the hybrid stars get soon unstable after formation of the tiny quark core. Nonetheless twin stars somehow manage to restabilize again at a higher transition pressure.

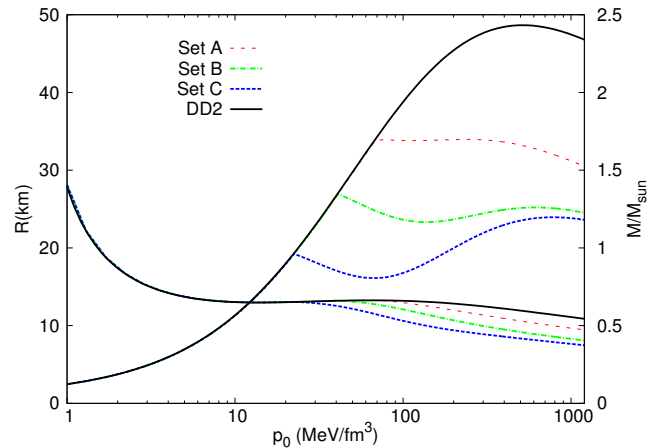


FIG. 19. *The radius- and mass curves for three different parameter sets corresponding to a QM-EoS given by eq. 11. The parameters of the three sets are displayed in tab. I. Set C shows the appearance of a second stable branch, where $M_2 > M_1$. All displayed solutions are twin star solutions. The curves starting in the upper left region are the radius curves whereas the curves starting on the lower left side are the mass curves.*

We do not get maximum mass values of the twin star configurations which are above the observational known value of $M = 2.01M_\odot$, which means as a consequence, that all the twin star EoS are ruled out by nature.

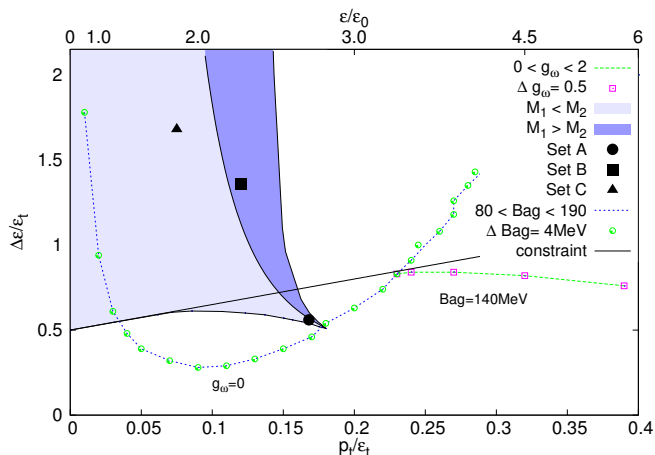


FIG. 20. Phase diagram for hybrid stars with the $g_\omega = 0$ -line and various values of B , and $B = 140$ MeV at various g_ω , both with $m_\sigma = 600$ MeV and $m_q = 300$ MeV. The axes display the transition pressure p_t and the energy density discontinuity $\Delta\epsilon$ in units of the nuclear energy density at the transition ϵ_t . The shaded regions displays the twin star regions with either $M_1 < M_2$ (light blue) or $M_1 > M_2$ (blue) calculated with the QM-EoS given by eq. 11. The three twin star parameters sets are labelled as Set A, Set B and Set C.

In Fig. 20 the twin star region in the model utilized by Alford et. al [20–22] is compared with the space of available parameters within our model. It can be easily seen that the main part of the region where twin stars exist lies out of our attainable values of $\Delta\epsilon/\epsilon_t$ and p_t/ϵ_t . Solely for irrelevant low values of p_t/ϵ_t we find a twin star area, see figure 14. The cusp at the lower end of the twin star region at $(p_t/\epsilon_t = 0.18, \Delta\epsilon/\epsilon_t = 0.51)$ overlaps in a tiny region with the curve for $g_\omega = 0$, however, we do not find any twin star in this parameter range. The radius-mass properties of hybrid stars near to the parameter region of the cusp, almost reach a twin-like structure (see e.g. the curve with $B = 120$ MeV in fig. 15), though they never accomplish it mathematically. The reason for this apparent contradiction is causally determined in the fact that the sound speed for $g_\omega = 0$ is not constant and slightly below the value which has been chosen to calculate the twin star area (see fig. 12). As pointed out in [20], a decrease of c_s^2 has the effect of scaling down the size of the twin star area and moves the cusp at the end of the twin star region upwards. Therefore, the absence of twin stars at the intersection of the cusp region is due to the energy dependence of the sound speed, which lowers its average value below $c_s^2 = 1/3$. The line between the shaded areas separates whether the mass of the first branch M_1 lies above (blue) or below (lighter blue) the mass of the second stable branch M_2 . The $g_\omega = 0$ line with $B = 120 - 124$ MeV gets closest to the twin star region.

Nevertheless, twin stars in general could exist in nature, as other models have been constructed [55, 56] that satisfy the $M^{max} > 2.01M_\odot$ constraint.

VI. CONCLUSIONS

In this work we employ a density dependent hadronic matter EoS and a density dependent chiral quark matter EoS to find the phase transition from one phase to the other within compact stars. The quarks couple to the meson fields via Yukawa-type interaction terms. We utilize a Maxwell construction, i.e. assume that there is a sharp transition at a given transition pressure. The transition pressure is identified when the chemical potential equals the pressure, from that point on the dominance in the EoS flips and the larger energy density from the QM EoS prevails. Within our parameter range we found stable hybrid star solutions and investigated the relation of the QM core size and the appropriate stability of the star. In the SU(3) Quark Meson model utilized for the QM EoS four parameters can be varied, from whom two of them (m_σ and m_q) have little effect on the results. We conclude that a larger repulsive coupling g_ω and a larger vacuum pressure B do not allow for a large QM core to appear but reach the $2M_\odot$ limit, whereas small values of both quantities generate hybrid star solutions with a corresponding, large QM core, but the configurations stay below the $2M_\odot$ constraint. Hybrid stars with high transition pressures are hard to distinguish from pure hadronic stars because of the tiny QM core. An appearing QM core generates an additional gravitational pull on the hadronic mantle. If the cores pressure can counteract this extra pull, the star is stable. For a too large discontinuity in energy density the star gets unstable since the pressure of the core is not able to counteract the extra gravitational pull [20–22]. In [20] Alford et. al use hadronic EoSes based upon works from Heberler et. al [57] and Shen et. al [58]. Their QM EoS is density independent and is parametrized through p_t , ϵ_t and, assuming a constant speed of sound, c_s^2 . They conclude that for stars with at least $2M_\odot$ a larger c_s^2 is advantageous, whereas for $c_s^2 = 1/3$ a larger region in the phase diagram for stars with $\geq 2M_\odot$ is excluded, which as a consequence restricts the other parameters p_t and ϵ_t . In a proximate work Alford et. al [21] apply the constant speed of sound parametrization to a Field-Correlator-Method calculation. The corresponding EoS is equipped with an additive density independent $\bar{q}q$ -potential, corresponding to our density dependent vector coupling constant, and with a vacuum energy density term including gluon condensate contributions, analogous to the Bag constant utilized in our approach. Vacuum energy density term and Bag constant are in both cases additive, i.e. density independent. In both works the allowed region in the phase diagram for hybrid stars with more than two solar masses is shifted to high transition pressures at several times nuclear energy density ($3.5 \leq \epsilon/\epsilon_0 \leq 6.5$). The family of the Field Correlator Method EoSes (varying the two above mentioned quantities) covers only a limited region in the phase diagram due to a nearly density independent speed of sound ($c_s^2 \simeq 1/3$), whereas in our approach we achieved high transition pressures as-

suming a higher vector coupling constant. This feature on the other hand raises the speed of sound up to values $c_s^2 \sim 0.6$, which would leave space in the phase diagram for the other parameters p_t and ϵ_t , only we had no direct influence on them. However, we confirm the results Alford et. al [20–22] obtained and investigate further why we were not able to find a third family (twin stars) of compact stars within a physically meaningful parameter region. The conclusion is that the chances for twins are best when the transition pressure is relatively low and the energy density discontinuity on the other hand relatively high, then an appearing QM core does not destabilize the star immediately. Likewise it gets harder to achieve the $2M_\odot$ regime. But if the discontinuity in energy density is too large, the pressure of the QM core is unable to counteract the additional downward pull and the star configurations becomes unstable. A future work could study the interplay between hadronic- and quark matter EoS in greater detail to work out how to achieve the ap-

propriate proportions between pressure and discontinuity in energy density for twin stars.

ACKNOWLEDGMENTS

The authors thank Laura Tolos and David Blaschke for discussions during the initial stage of this project. Furthermore we want to thank Thorben Graf and Rainer Stiele for helpful suggestions during the whole project. We gratefully acknowledge Sophia Han and Mark Alford for pointing out an inconsistency in the twin star area region of the previous version of our article and additionally want to thank them for further remarks. AZ is supported by the Helmholtz Graduate School for Heavy-Ion Research (HGS-HIRE) and the Helmholtz Research School for Quark Matter (H-QM). MH gratefully acknowledges support from the Frankfurt Institute for Advanced Studies (FIAS).

-
- [1] P. Demorest, T. Pennucci, S. Ransom, M. Roberts, and J. Hessels, *Nature* **467**, 1081 (2010), arXiv:1010.5788 [astro-ph.HE].
- [2] J. Antoniadis, P. C. Freire, N. Wex, T. M. Tauris, R. S. Lynch, M. H. van Kerkwijk, M. Kramer, C. Bassa, V. S. Dhillon, T. Driebe, J. W. T. Hessels, V. M. Kaspi, V. I. Kondratiev, N. Langer, T. R. Marsh, M. A. McLaughlin, T. T. Pennucci, S. M. Ransom, I. H. Stairs, J. van Leeuwen, J. P. W. Verbiest, and D. G. Whelan, *Science* **340**, 6131 (2013), arXiv:1304.6875 [astro-ph.HE].
- [3] R. A. Hulse and J. H. Taylor, *Astrophys. J.* **195**, L51 (1975).
- [4] J. Zdunik and P. Haensel, *Astron.Astrophys.* **551**, A61 (2013), arXiv:1211.1231 [astro-ph.SR].
- [5] R. C. Tolman, *Relativity, Thermodynamics and Cosmology* (Oxford University Press, Oxford, 1934).
- [6] I. Sagert, M. Hempel, C. Greiner, and J. Schaffner-Bielich, *Eur.J.Phys.* **27**, 577 (2006), arXiv:astro-ph/0506417 [astro-ph].
- [7] N. Itoh, *Prog.Theor.Phys.* **44**, 291 (1970).
- [8] A. R. Bodmer, *Phys. Rev. D* **4**, 1601 (1971).
- [9] E. Witten, *Phys. Rev. D* **30**, 272 (1984).
- [10] A. Zacchi, R. Stiele, and J. Schaffner-Bielich, (2015), arXiv:1506.01868 [astro-ph.HE].
- [11] B. Kämpfer, *Phys. Lett.* **101B**, 366 (1981).
- [12] B. Kämpfer, *J. Phys. A* **14**, L471 (1981).
- [13] B. Kämpfer, *Astron. Nachr.* **303**, 231 (1982).
- [14] B. Kämpfer, *J. Phys. A* **16**, 633 (1983).
- [15] B. Kämpfer, *Astron. Nachr.* **304**, 167 (1983).
- [16] B. Kämpfer, *Phys. Lett.* **153B**, 121 (1985).
- [17] N. K. Glendenning and C. Kettner, *Astron. Astrophys.* **353**, L9 (2000), astro-ph/9807155.
- [18] K. Schertler, C. Greiner, J. Schaffner-Bielich, and M. H. Thoma, *Nucl. Phys.* **A677**, 463 (2000), arXiv:astro-ph/0001467 [astro-ph].
- [19] D. Blaschke and D. E. Alvarez-Castillo, (2015), arXiv:1503.03834 [astro-ph.HE].
- [20] M. G. Alford, S. Han, and M. Prakash, *JPS Conf.Proc.* **1**, 013041 (2014).
- [21] M. G. Alford, G. Burgio, S. Han, G. Taranto, and D. ZappalÀ, (2015), arXiv:1501.07902 [nucl-th].
- [22] M. G. Alford and S. Han, (2015), arXiv:1508.01261 [nucl-th].
- [23] S. Typel, G. Röpke, T. Klähn, D. Blaschke, and H. H. Wolter, *Phys. Rev.* **C81**, 015803 (2010), arXiv:0908.2344 [nucl-th].
- [24] Z. Fodor and S. D. Katz, *JHEP* **03**, 014 (2002), arXiv:hep-lat/0106002.
- [25] Z. Fodor, *PoS CPOD07*, 027 (2007), arXiv:0712.2930 [hep-lat].
- [26] D. Alvarez-Castillo and D. Blaschke, (2013), arXiv:1304.7758 [astro-ph.HE].
- [27] N. K. Glendenning, *Phys.Rev.* **D46**, 1274 (1992).
- [28] A. Bhattacharyya, S. K. Ghosh, M. Hanauske, and S. Raha, astro-ph/0406509 (2004).
- [29] A. Bhattacharyya, I. N. Mishustin, and W. Greiner, *J.Phys.* **G37**, 025201 (2010), arXiv:0905.0352 [nucl-th].
- [30] V. Koch, *Int. J. Mod. Phys.* **E6**, 203 (1997), nucl-th/9706075.
- [31] N. A. Törnqvist, hep-ph/9711483 (1997).
- [32] J. T. Lenaghan, D. H. Rischke, and J. Schaffner-Bielich, *Phys.Rev.* **D62**, 085008 (2000), arXiv:nucl-th/0004006 [nucl-th].
- [33] D. Parganlija, P. Kovacs, G. Wolf, F. Giacosa, and D. Rischke, *AIP Conf.Proc.* **1520**, 226 (2013), arXiv:1208.5611 [hep-ph].
- [34] B.-J. Schaefer and M. Wagner, *Phys. Rev.* **D79**, 014018 (2009), arXiv:0808.1491 [hep-ph].
- [35] D. Parganlija, F. Giacosa, and D. H. Rischke, *Phys.Rev.* **D82**, 054024 (2010), arXiv:1003.4934 [hep-ph].
- [36] K. Olive *et al.* (Particle Data Group), *Chin.Phys.* **C38**, 090001 (2014).
- [37] K. Schertler, S. Leupold, and J. Schaffner-Bielich, *Phys.Rev.* **C60**, 025801 (1999),

- arXiv:astro-ph/9901152 [astro-ph].
- [38] T. Maruyama, T. Tatsumi, T. Endo, and S. Chiba, *Recent Res.Devel.Phys.* **7**, 1 (2006), arXiv:nucl-th/0605075 [nucl-th].
- [39] M. Hempel, V. Dexheimer, S. Schramm, and I. Iosilevskiy, *Phys. Rev.* **C88**, 014906 (2013), arXiv:1302.2835 [nucl-th].
- [40] Z. Seidov, *Sov. Astron.* 15 (347) (1971).
- [41] B. Kämpfer, *J. Phys. G* **9**, 1487 (1983).
- [42] Z. L. Schaeffer, R. and P. Haensel, *Astron. Astrophysics*, 126 (121-145) (1983).
- [43] L. Lindblom, *Phys.Rev.* **D58**, 024008 (1998), arXiv:gr-qc/9802072 [gr-qc].
- [44] S. L. Shapiro and S. A. Teukolsky, *Black Holes, White Dwarfs, and Neutron Stars: The Physics of Compact Objects* (John Wiley & Sons, New York, 1983).
- [45] N. K. Glendenning, *Compact Stars: Nuclear Physics, Particle Physics and General Relativity* (Springer, Berkeley, 1997).
- [46] P. Ko and S. Rudaz, *Phys.Rev.* **D50**, 6877 (1994).
- [47] T. Beisitzer, R. Stiele, and J. Schaffner-Bielich, *Phys.Rev.* **D90**, 085001 (2014), arXiv:1403.8011 [nucl-th].
- [48] I. Mishustin, M. Hanauske, A. Bhattacharyya, L. Satarov, H. Stoecker, *et al.*, *Phys.Lett.* **B552**, 1 (2003), arXiv:hep-ph/0210422 [hep-ph].
- [49] M. Hanauske, .
- [50] J. Schaffner-Bielich, M. Hanauske, H. Stoecker, and W. Greiner, *Phys.Rev.Lett.* **89**, 171101 (2002).
- [51] B. Kämpfer, *J.Phys.* **A14**, L471 (1981).
- [52] S. Banik, M. Hanauske, D. Bandyopadhyay, and W. Greiner, arXiv:astro-ph/0406315 (2004).
- [53] S. Banik, M. Hanauske, and D. Bandyopadhyay, *J.Phys.* **G31**, S841 (2005), arXiv:nucl-th/0412110 [nucl-th].
- [54] J. Zdunik and P. Haensel, *Astronomy & Astrophysics* **551**, A61 (2013).
- [55] S. Benic, D. Blaschke, D. E. Alvarez-Castillo, T. Fischer, and S. Typel, *Astron.Astrophys.* **577**, A40 (2015), arXiv:1411.2856 [astro-ph.HE].
- [56] V. Dexheimer, R. Negreiros, and S. Schramm, *Phys.Rev.* **C91**, 055808 (2015), arXiv:1411.4623 [astro-ph.HE].
- [57] K. Hebeler, J. Lattimer, C. Pethick, and A. Schwenk, *Phys.Rev.Lett.* **105**, 161102 (2010), arXiv:1007.1746 [nucl-th].
- [58] G. Shen, C. J. Horowitz, and S. Teige, *Phys. Rev.* **C83**, 035802 (2011), arXiv:1101.3715 [astro-ph.SR].